Molecularly Engineered Biodegradable Polymer Networks with a Wide Range of Stiffness for Bone and Peripheral Nerve Regeneration

Shanfeng Wang, Diederik H. R. Kempen, Godard C. W. de Ruiter, Lei Cai, Robert J. Spinner, Anthony J. Windebank, Michael J. Yaszemski, and Lichun Lu**

To satisfy different mechanical requirements in hard and soft tissue replacements, a series of biodegradable and crosslinkable copolymers of poly(propylene fumarate)-*co*-polycaprolactone (PPF-*co*-PCL) are synthesized and employed to fabricate 2D disks and 3D scaffolds via photocrosslinking. Thermal properties such as the glass transition temperature (T_g) and melting temperature (T_m) of the PPF-*co*-PCL networks can be controlled efficiently by varying the PCL composition (ϕ_{PCL}). As a result, their mechanical properties vary significantly from hard and stiff materials to soft and flexible ones with increasing ϕ_{PCL}, making them attractive candidate materials for bone and peripheral nerve regeneration, respectively. Several PPF-*co*-PCL formulations are selected to perform in vitro cell studies using mouse pre-osteoblastic MC3T3-E1, rat Schwann cell precursor line (SPL201), and pheochromocytoma (PC12) cells, and in vivo animal testing in the rat femur bone defect model and in the rat sciatic nerve transection model. The formation of new bone in the porous bone scaffolds with a low ϕ_{PCL} and guided axon growth through the nerve conduits with a higher ϕ_{PCL} suggest that crosslinked PPF-*co*-PCLs have appropriate compatibility and functionality. Furthermore, the role of surface stiffness in modulating cellular behavior and functions is verified on the crosslinked PPF-*co*-PCL surfaces without any pretreatments.

1. Introduction

Tissue engineering requires biomaterials with sufficient and appropriate mechanical properties for diverse applications such as hard-tissue and soft-tissue replacements. Meanwhile, the controllability of material properties is critical in investigating cell–biomaterial interactions. In this report, we present a series of novel crosslinkable polymeric biomaterials with a wide range of controllable physicochemical properties as candidate materials for bone and peripheral nerve regeneration.

The clinical needs for bone regeneration include bone defects that occur after resection of primary and metastatic tumors, bone loss after skeletal trauma, and trabecular voids following osteoporotic insufficiency fractures.[1,2] Current clinical treatments include autograft and allograft bone, nondegradable poly(methyl methacrylate) (PMMA), and synthetic bone graft substitutes. Disadvantages associated with these options include a limited supply and donor site morbidity in the case of autografts, and a risk of disease transfer in the case of allograft bone. PMMA can cause tissue damage secondary to the high temperature generated during the reaction, stress shielding, particulate wear, and leachable toxic small molecules after the polymerization.[1,2] Another challenging clinical problem considered in this study is injury to peripheral nerves. Presently the "gold standard" for repairing an injured peripheral nerve is an autologous nerve graft.[3,4] The disadvantages associated with autologous nerve grafting include limited sources of donor nerve, the need of a second surgery to obtain the donor nerve, loss of function in the sensory distribution of the donor nerve, and size mismatch between the injured nerve and the donor nerve.[3,4]

Synthetic biodegradable polymers are excellent replacement materials because of their unlimited supply, minimum risk of disease transfer, and reproducible chemical, physical, and biologic properties, and the possibility of coupling the polymer degradation rate with the tissue regeneration rate. Polymers of this kind have been used to fabricate porous bone scaffolds to encourage bone growth into contained and segmental skeletal defects,[1,2] and nerve conduits to bridge the gap between segmental peripheral nerve injuries.[3,4] The polymeric materials

Prof. S. Wang, Dr. L. Cai
Department of Materials Science and Engineering
The University of Tennessee
Knoxville, TN 37996, USA
E-mail: swang16@utk.edu
Dr. D. H. R. Kempen, Prof. R. J. Spinner,
Prof. M. J. Yaszemski, Prof. L. Lu
Department of Orthopedic Surgery
Mayo Clinic College of Medicine
Rochester, MN 55905, USA
E-mail: lu.lichun@mayo.edu
Prof. M. J. Yaszemski, Prof. L. Lu
Department of Physiology and Biomedical Engineering
Mayo Clinic College of Medicine
Rochester, MN 55905, USA
Dr. G. C. W. de Ruiter, Prof. R. J. Spinner
Department of Neurologic Surgery
Mayo Clinic College of Medicine
Rochester, MN 55905, USA
Prof. A. J. Windebank
Department of Neurology
Mayo Clinic College of Medicine
Rochester, MN 55905, USA

DOI: 10.1002/adfm.201500105

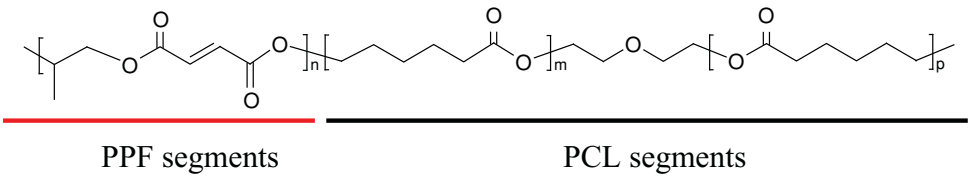

Figure 1. Chemical structure of PPF-*co*-PCL.

should satisfy general requirements such as appropriate swelling behavior and biodegradation rate, feasibility of fabrication, and sterilizability. In addition, they should satisfy requirements specific to the particular application for which they were designed, such as mechanical properties, selective cell migration and attachment, and tissue-specific biocompatibility.[1,3] The concept of the common hollow or single lumen nerve conduit has been modified by incorporating Schwann cells, growth factors, guiding filaments, and microarchitectures such as multiple channels.[3,4] Compared to single lumen nerve conduits, multichannel nerve conduits provide more luminal surface area per volume for cell attachment and controlled release of incorporated growth factors.

We have synthesized and extensively characterized novel crosslinkable and biodegradable poly(propylene fumarate)-*co*-poly(ε-caprolactone) (PPF-*co*-PCL) copolymers with 15 compositions (**Figure 1**).[5] The glass transition temperature (T_g) and the density of crosslinkable or unsaturated PPF segments both decrease as the percentage of saturated PCL (ϕ_{PCL}) increases in the composite formulation.[5] After crosslinking, the thermal properties, mechanical properties, and biodegradation rate vary in a systematic manner based on ϕ_{PCL}. Thus, crosslinked PPF-*co*-PCLs demonstrate a wide range of physical properties that lie between those for crosslinked PPF[6] and PCL. We report here the controllability in photocrosslinking characteristics using PPF-*co*-PCLs with various compositions, in vitro cell studies and in vivo animal studies. The mechanical properties of elastic substrates have been shown to regulate cell behavior.[7–23] This report also emphasizes the modulation of in vitro bone and nerve cell behavior by the controlled polymeric scaffold's physical properties, particularly surface stiffness, and the role of mechanical properties in selecting appropriate materials for bone scaffolds and nerve conduits used in vivo. We demonstrate the correlation of cellular responses to scaffold molecular design.

2. Results and Discussion

The PPF-*co*-PCLs in this study had a wide range of physical properties before and after crosslinking.[5] The crosslinking step permits the preparation of prepolymers that have specific properties which determine the final properties of the crosslinked network. These prepolymers serve as the starting materials for polymer processing into the desired devices for the intended clinical application.[5] The gel fractions of photocrosslinked PPF-*co*-PCL disks were all close to 100%, indicating that the density of crosslinkable segments and the crosslinking conditions were sufficient for forming homogeneous polymer networks. No significant heat release (the maximum temperature was ≈37 °C) occurred during the crosslinking of PPF-*co*-PCLs. This was true for crosslinking reactions that began with either the photocrosslinking initiator phenyl bis(2,4,6-trimethyl benzoyl) phosphine oxide (BAPO) or the redox crosslinking system consisting of the initiator benzoyl peroxide and the accelerator *N*-dimethyl toluidine. Because the presence of PCL blocks in the PPF-*co*-PCL copolymers decreased the density of crosslinking, the swelling ratio of the crosslinked polymer network [Figure S1, Supporting Information] in methylene chloride (CH_2Cl_2), which is a good solvent for both PCL and PPF, increased greatly from 34% to 390% as ϕ_{PCL} increased from 30% to 90%. The swelling ratio also increased from 6% to 27% in ethanol. Crosslinked PPF-*co*-PCLs were hydrophobic; thus, little swelling (swelling ratios < 5%) was detected in phosphate buffered saline (PBS) solution, which is advantageous for surgical implantation as no distortion of the scaffold shape or change in its designed dimensions will result from swelling.

As depicted in **Figure 2**A, PCL is a semicrystalline polymer with a molecular weight-dependent crystallinity that varies from ≈30% to 60%.[5] PPF-*co*-PCLs had lower crystallinities because the PPF blocks were amorphous.[5] After crosslinking, the crosslinks further suppressed the crystalline domains and reduced both the percent crystallinity and the melting temperature (T_m). The crystalline domains can be considered as physical fillers that enhance the network mechanical properties when the copolymer networks are semicrystalline. The heating differential scanning calorimetry (DSC) curves of the crosslinked PPF-*co*-PCLs in Figure 2B demonstrated a single glass transition for $\phi_{PCL} \leq 87\%$, indicating that the networks were amorphous up to this composition. The glass transition broadened and shifted to a higher temperature when ϕ_{PCL} decreased, because T_g of PCL (−68.3 °C) was much lower than that of PPF (24.2 °C). Thermal properties such as T_g and T_m are plotted as functions of ϕ_{PCL} in Figure 2C with data from uncrosslinked PPF-*co*-PCLs for comparison. Crosslinking PPF-*co*-PCL increased its T_g because the crosslinks limited segmental motion. When the crosslink density reached a certain level, the glass transition disappeared completely. This occurred for PPF-*co*-PCL when $\phi_{PCL} \leq 31\%$, as demonstrated in Figure 2B. Among the 15 crosslinked PPF-*co*-PCLs, only the network with $\phi_{PCL} = 90\%$ had an exothermal peak at a cold crystallization temperature (T_{cc}) of −13.0 °C and an endothermal peak at T_m of 17.1 °C, and the heats of fusion (ΔH_m) calculated from the peak areas were 5.17 and 2.84 J g^{-1}, respectively. Both T_m and ΔH_m were significantly lower than 41.8 °C and 48.4 J g^{-1} that occurred in its uncrosslinked form.[5] In turn, the PCL diol precursor for synthesizing PPF-*co*-PCL (ϕ_{PCL} = 90%) had higher values for the crystalline peak (48.7 °C) and the heat of fusion (ΔH_m = 76.7 J g^{-1}).[5] In contrast, the DSC curve of crosslinked PPF-*co*-PCL (ϕ_{PCL} = 90%) collected from the cooling run (Figure S2A, Supporting Information) did not show any

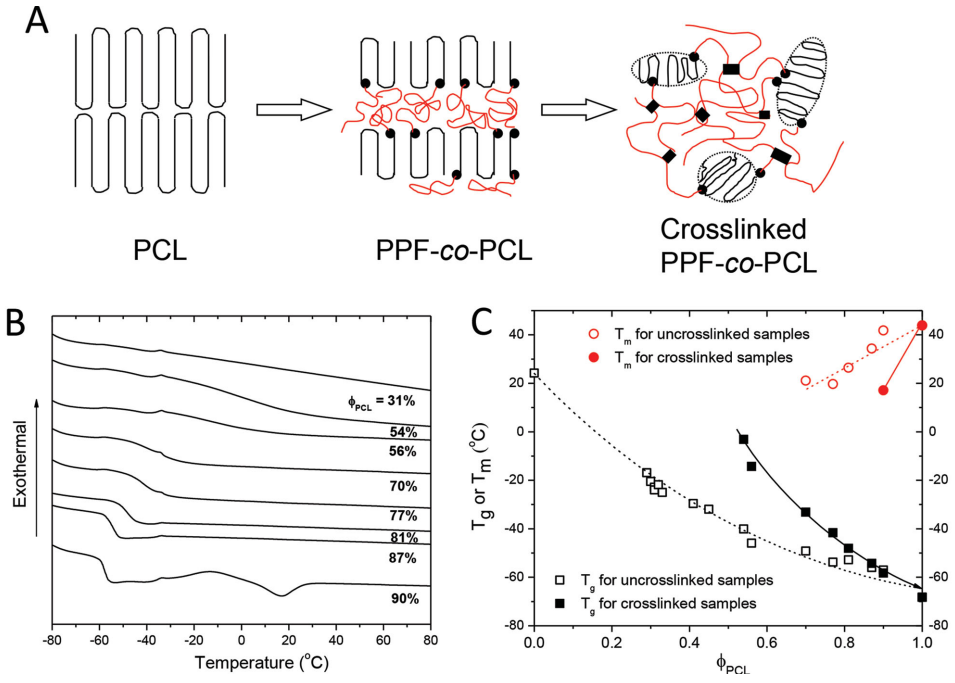

Figure 2. Thermal properties of crosslinked PPF-*co*-PCLs. A) Schematic illustration of the morphological change in copolymerization (step 1: PCL → PPF-*co*-PCL) and crosslinking (step 2: PPF-*co*-PCL → crosslinked PPF-*co*-PCL) at temperature lower than T_m. PCL segments in black and PPF segments in red are connected with round dots in PPF-*co*-PCL and PPF segments are further linked with crosslinks (thick rods) in crosslinked PPF-*co*-PCL. B) Heating DSC curves and C) T_g and T_m of crosslinked PPF-*co*-PCLs with different ϕ_{PCL}. T_g and T_m of uncrosslinked PPF-*co*-PCLs are included for comparison.

exothermal crystallization peak. The block length or the molecular weight of the PCL diol precursor was critical, especially when the synthesized PPF-*co*-PCL was semicrystalline, because a higher molecular weight PCL diol will result in a PPF-*co*-PCL that has a higher crystallinity and T_m at the same ϕ_{PCL}.[5]

Crystallinity and crosslinking density play correlative roles in determining the final mechanical properties of crystalline polymer networks.[19–24] In this study, only crosslinked PPF-*co*-PCL (ϕ_{PCL} = 90%) was semicrystalline. All other compositions were amorphous. Thus, although three nominal number-average molecular weights ($\bar{M}_n$) of PCL diol precursor (530, 1250, and 2000 g mol^{-1}) were used in synthesizing PPF-*co*-PCL, ϕ_{PCL} was the dominant factor in determining the mechanical properties of crosslinked PPF-*co*-PCLs for $\phi_{PCL} \leq 90\%$. The crosslinked network's tensile modulus increased dramatically (by a factor of ≈560) as ϕ_{PCL} decreased from 90% to zero: the modulus for crosslinked PPF-*co*-PCL (ϕ_{PCL} = 90%) was 2.68 ± 0.05 MPa and the modulus for crosslinked PPF (ϕ_{PCL} = 0%) was 1.5 ± 0.2 GPa, as shown in **Figure 3**A. Correspondingly, as ϕ_{PCL} decreased from 90% to zero, the strength at break increased from 0.89 to 28.1 MPa, and the elongation at break decreased from 43.2% to 2.6%. Thus, ϕ_{PCL} was an efficient parameter to use for modulation of the tensile properties of crosslinked PPF-*co*-PCLs from flexible characteristics at a high ϕ_{PCL} to rigid characteristics at a low ϕ_{PCL}. Furthermore, the mechanical properties calculated for crosslinked PPF-*co*-PCLs in this study are in good agreement with our previous results for blend networks consisting of PPF and poly(ε-caprolactone) fumarate (PCLF).[15,21]

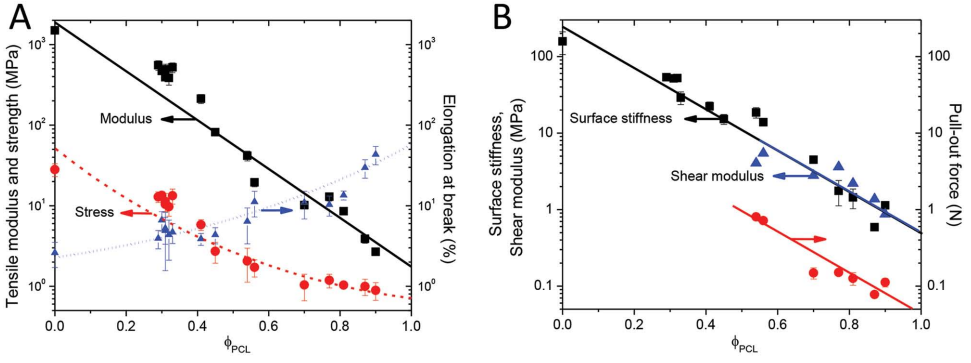

Figure 3. A) Tensile characteristics at room temperature and B) surface stiffness (■) at room temperature, shear modulus (▲) at 37 °C, pull-out force (●) at room temperature of crosslinked PPF-*co*-PCLs with different ϕ_{PCL}.

The material design strategy presented in this report offers a wide range of mechanical properties for diverse applications in hard and soft tissue replacements. The tensile properties of crosslinked PPF-*co*-PCL with ϕ_{PCL} lower than 54% were comparable to those of trabecular bone (50 MPa–0.5 GPa for tensile modulus, 10–20 MPa for tensile strength at break, and 5%–7% for elongation at break), though the tensile modulus and strength at break were lower than those of cortical bone (14–20 GPa and 50–150 MPa, respectively).[25] The tensile properties of crosslinked PPF-*co*-PCLs with ϕ_{PCL} higher than 81% were comparable to those of a freshly transected, coapted, and sutured adult rat sciatic nerve (4 MPa for tensile modulus, 0.78 MPa for strength at break, and 30% for elongation at break).[26] We propose that the rigid and strong crosslinked PPF-*co*-PCLs (low ϕ_{PCL}) are appropriate candidate bone scaffold materials, while the soft and flexible ones (high ϕ_{PCL}) are appropriate for guiding axon growth in peripheral nerve regeneration.

Figure 3B shows that the surface stiffness, shear modulus, and pull-out force of crosslinked PPF-*co*-PCL samples can also be modulated by varying ϕ_{PCL}. The shear modulus was measured at a frequency of 1 rad s^{-1} and a temperature of 37 °C, while other mechanical characteristics were measured at room temperature. The pull-out force test is a measure of the material's capability to resist tearing and to hold sutures during its implantation.[15] When ϕ_{PCL} was lower than 54%, crosslinked PPF-*co*-PCL disks were no longer suturable. Thus, no shear and pull-out experiments were conducted on these rigid samples. Interestingly, three mechanical characteristics appeared to share the same ϕ_{PCL} dependence. Surface stiffness increased from 1.1 ± 0.12 MPa for crosslinked PPF-*co*-PCL (ϕ_{PCL} = 90%) to 158 ± 52 MPa for crosslinked PPF (ϕ_{PCL} = 0). When ϕ_{PCL} decreased from 90% to 54%, shear modulus and pull-out force also increased from 0.87 MPa and 0.11 N to 4.0 MPa and 0.80 N, respectively. Note that the shear modulus of crosslinked PPF-*co*-PCL (ϕ_{PCL} = 90%) was lower than that for crosslinked PPF-*co*-PCL (ϕ_{PCL} = 87%) because both were amorphous at 37 °C while the latter had a higher density of crosslinking. At room temperature, crystallites were present in specimens made from both these compositions, and the surface stiffness and pull-out force measurements demonstrated opposite trends compared to those measured at 37 °C. For crosslinked PPF-*co*-PCL (ϕ_{PCL} = 90%) nerve conduits (1.98 mm, average outer diameter; 11.1–12.7 mm, length), the flexural modulus was 52.0 ± 1.2 MPa for single-channel conduits and 66.0 ± 3.7 MPa for seven-channel conduits, which were comparable to the value of 73.4 ± 12.7 MPa for crosslinked PCLF single-lumen conduits that have a ϕ_{PCL} of 98.1%, crystallinity of 37%, and T_m of 42 °C.[27]

The physical properties of crosslinked PPF-*co*-PCL (ϕ_{PCL} = 90%) can be further modulated by the weight ratio of the photoinitiator BAPO to the PPF-*co*-PCL in the crosslinking recipe. The crosslinking density was reported to be lower at a smaller BAPO/PCLF ratio, and resulted in a higher crystallinity and T_m in the produced polymer network.[21] Distinct from the cooling DSC curve (Figure S2A, Supporting Information) for crosslinked PPF-*co*-PCL (ϕ_{PCL} = 90%) at the BAPO/PPF-*co*-PCL ratio of 10 mg g^{-1}, an exothermal peak with ΔH_m of 11.6 J g^{-1} appeared at a crystallization temperature (T_c) of −24.0 °C when the ratio decreased to 1.67 mg g^{-1}. In the heating curves (Figure S2B, Supporting Information), T_m and ΔH_m were both higher (23.1 °C and 24.7 J g^{-1}) at the ratio of 1.67 mg g^{-1} compared to 17.1 °C and 2.84 J g^{-1} at 10 mg g^{-1} and a larger exothermal crystallization peak (ΔH_m of 13.0 J g^{-1}) appeared at a lower T_{cc} of −20.0 °C. Due to the presence of prominent crystalline domains when the BAPO/PPF-*co*-PCL ratio decreased from 10 to 1.67 mg g^{-1}, the tensile modulus for crosslinked PPF-*co*-PCL (ϕ_{PCL} = 90%) increased ≈55 times to 148 ± 35 MPa and the pull-out force increased approximately three times to 0.34 ± 0.02 N at room temperature.

The presence of ester bonds in crosslinked PPF-*co*-PCLs renders them degradable via hydrolysis. Degradation profiles were measured for crosslinked PPF-*co*-PCL disks that had diameters of 5 mm, thicknesses of 0.34 mm, and initial weights of ≈0.02 g. The weight change over time was examined in both PBS and 1 N NaOH aqueous solution at 37 °C. No apparent degradation occurred in PBS over the one week time period during which the in vitro cell studies were performed. The degradation profile (Figure S3, Supporting Information) in both PBS and 1 N NaOH solution could be modulated by varying the ϕ_{PCL}, and the degradation rate increased gradually with increasing ϕ_{PCL}. In PBS, the weight decrease was 6%–22% after 35 weeks and 15%–30% after 71 weeks. The degradation of crosslinked PPF-*co*-PCLs was significantly faster in 1 N NaOH solution, in which all samples degraded completely within six weeks. Crosslinked PPF-*co*-PCL (ϕ_{PCL} = 90%) had the highest degradation rate, with little residue remaining after one week.

Three PPF-*co*-PCLs with ϕ_{PCL} of 31%, 70%, and 90% were chosen to fabricate 2D crosslinked disks for performing cell studies. The weight-average molecular weight ($\bar{M}_w$) and $\bar{M}_n$ of these three PPF-*co*-PCLs with ϕ_{PCL} of 31%, 70%, and 90% were 4030 and 8230, 8570 and 18 300, and 14 200 and 28 600 g mol^{-1}, respectively.[5] Mouse MC3T3-E1 pre-osteoblastic cells, rat Schwann cell precursor line (SPL201) cells that are for myelinating axons,[28] and rat pheochromocytoma (PC12) cells that can be induced by nerve growth factor (NGF) into a neuronal phenotype were used to evaluate the material's biocompatibility for bone and nerve regeneration. Exemplified using SPL201 cells (Figure S4, Supporting Information), cell viability was found to be close to 100% when exposed to the crosslinked PPF-*co*-PCL disks for the same seven-day time period, compared to the same cells grown on tissue culture polystyrene (TCPS) as a positive control. The cytocompatibility results suggest that no toxic leachable molecules were released from the crosslinked PPF-*co*-PCL disks in seven days.

The fluorescence microscopic images and data that demonstrate cell morphology behavior, attachment, spreading, and proliferation on crosslinked PPF-*co*-PCL disks are presented in **Figure 4** and Figures S5–S8, Supporting Information. Evidently, the substrate composition played a key role in regulating cell behavior for all these three cell types. Furthermore, such composition-dependent phenomena in MC3T3-E1 and SPL201 cells were similar while they were different from those in PC12 cells. MC3T3-E1 and SPL201 cell attachment (Figure S5, Supporting Information) at 4 h postseeding normalized to the values of TCPS decreased significantly with increasing the ϕ_{PCL} in the substrates while PC12 cells did not vary with ϕ_{PCL}. Figure 4A shows cell morphology at four or seven days postseeding onto the crosslinked PPF-*co*-PCL (ϕ_{PCL} = 31%, 70%, and 90%) disks

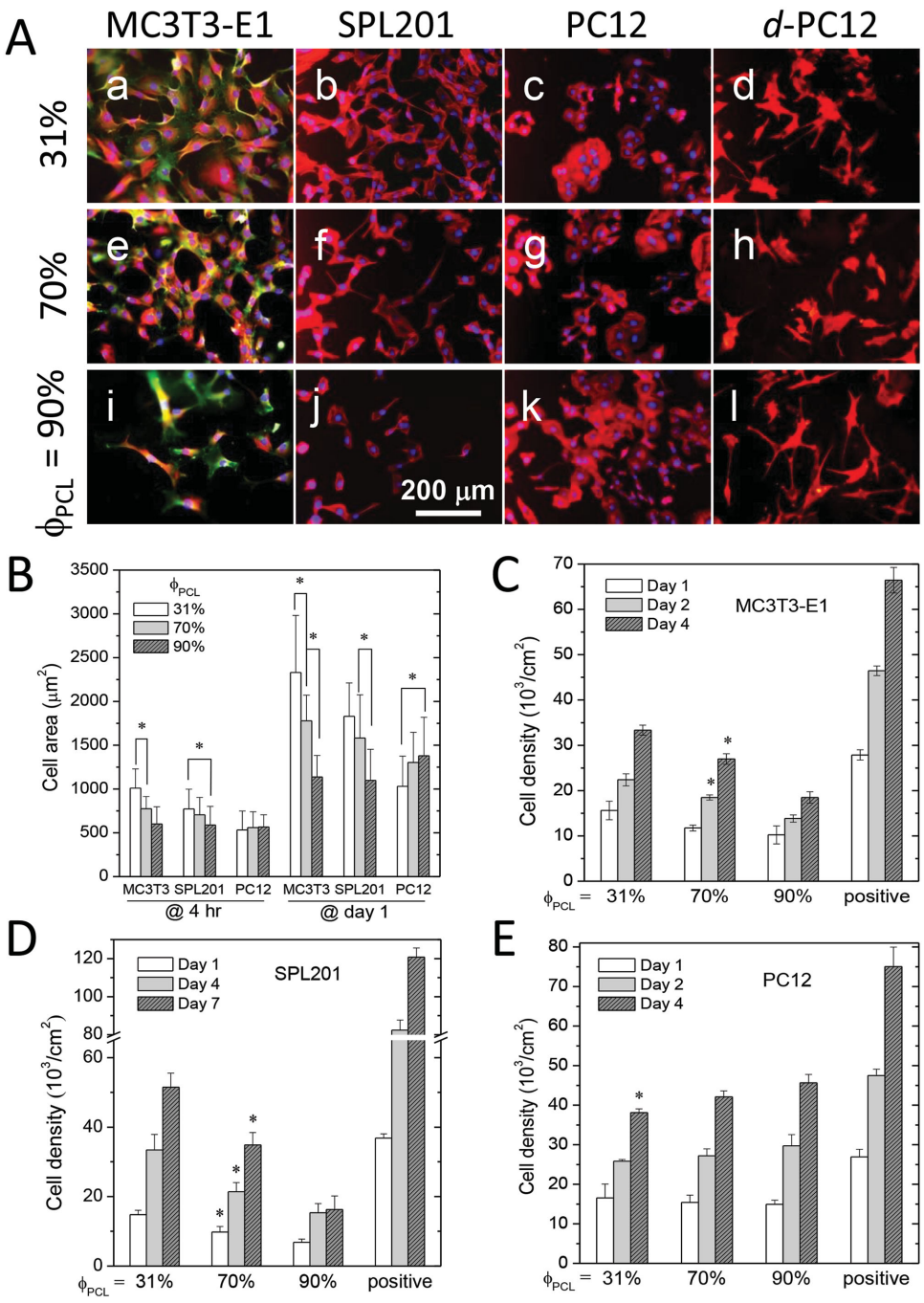

Figure 4. Cell behavior on crosslinked PPF-*co*-PCL substrates with ϕ_{PCL} of 31%, 70%, and 90%. A) Morphology (x100) of MC3T3-E1, SPL201, PC12, and differentiated PC12 (*d*-PC12) cells at days 4, 7, 4, and 7 postseeding, respectively. a–d) ϕ_{PCL} = 31%, e–h) ϕ_{PCL} = 70%, and i–l) ϕ_{PCL} = 90%. The scale bar of 200 μm in j) is applicable to all. Cytoplasm was stained red using rhodamine–phalloidin, vinculin was stained green using FITC, and cell nuclei was stained blue using DAPI. B) Average area of MC3T3-E1, SPL201, and PC12 cells. *$p < 0.05$ between different samples. Proliferation of C) MC3T3-E1, D) SPL201, and E) PC12 cells over four or seven days compared to cells seeded on TCPS (positive control). *$p < 0.05$ between the marked sample with another two samples at the same time point.

that had surface stiffnesses of 51.7 ± 3.1, 4.47 ± 0.39, and 1.14 ± 0.12 MPa, respectively. Crosslinked PPF-*co*-PCL (ϕ_{PCL} = 31%) disks supported MC3T3-E1 and SPL201 cell adhesion and proliferation efficiently: the cells were well-spread and adherent to the substrate with distinct actin fibers at all four time points (Figures S5–S8, Supporting Information). Focal adhesions were visualized by immune-staining for vinculin in MC3T3-E1 cells and more intensive vinculin staining in the cytoplasm was observed on crosslinked PPF-*co*-PCL (ϕ_{PCL} = 31%) compared to another two compositions. For MC3T3-E1 and SPL201 cells, the cell density decreased significantly and cell morphology became more rounded as ϕ_{PCL} increased. As summarized in

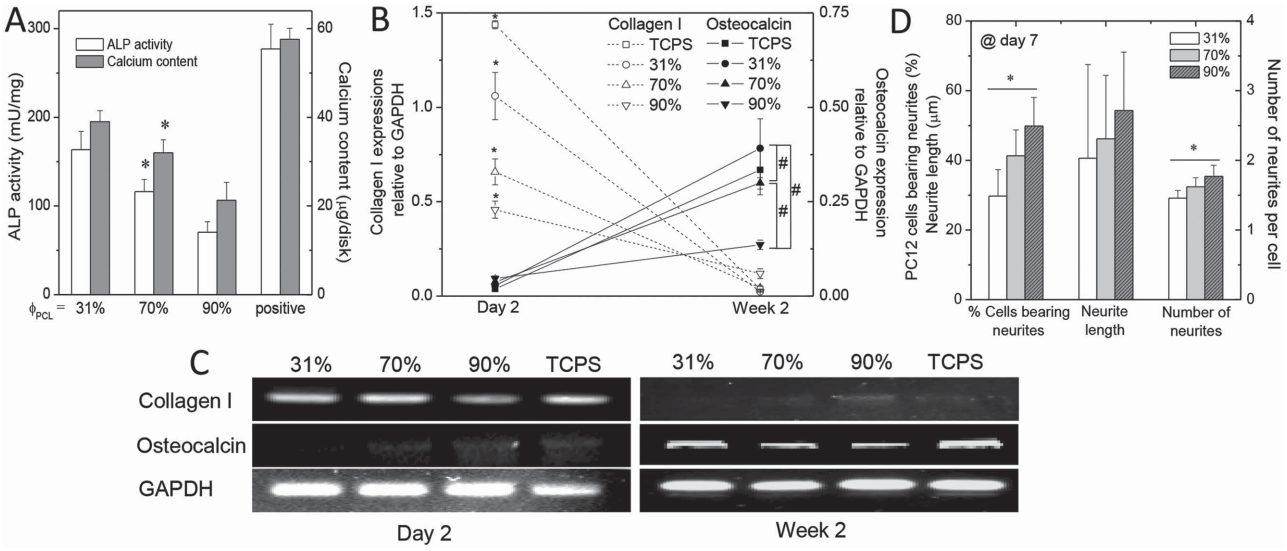

Figure 5. A) ALP activity and calcium content of MC3T3-E1 cells cultured on the crosslinked PPF-*co*-PCL disks with ϕ_{PCL} of 31%, 70%, and 90% for seven days, compared with TCPS positive control wells. $*p < 0.05$ between the marked sample with another two samples. B) Real-time PCR and C) RT-PCR analysis for characterizing gene expression levels of collagen I and osteocalcin normalized by that of GAPDH in MC3T3-E1 cells cultured on the crosslinked PPF-*co*-PCL disks and TCPS control wells for two days or two weeks. In B), $*p < 0.05$ between any two marked groups; $\#p < 0.05$ between two indicated groups. D) Percentage PC12 cells bearing neurites, neurite length, and number of neurites per cell on the crosslinked PPF-*co*-PCL disks with ϕ_{PCL} of 31%, 70%, and 90%. $*p < 0.05$ between different samples.

Figure 4B, cell area approximately doubled from 4 h to one day postseeding for all these three cell types. With increasing the ϕ_{PCL} in the substrates, the average areas of MC3T3-E1 and SPL201 cells decreased at both time points while PC12 cells did not demonstrate such dependence at 4 h and PC12 cell area even increased at day 1.

The corresponding cell numbers calculated from MTS adsorption data at three time points are given in Figure 4C–E to assess cell proliferation. Only slight cell proliferation occurred for MC3T3-E1 and SPL201 cells seeded onto the crosslinked PPF-*co*-PCL (ϕ_{PCL} = 90%) disks while a significant cell proliferation can be found for crosslinked PPF-*co*-PCL (ϕ_{PCL} = 31%) disks. Calculated by dividing the cell number at day 4 by the initial attached cell number at 4 h, the proliferation index (PI) of MC3T3-E1 cells decreased from 2.8 ± 0.2 to 2.5 ± 0.2 and then to 2.0 ± 0.2. The doubling time of MC3T3-E1 cells, defined as ln2/ln(PI) × 4, was prolonged from 2.7 ± 0.2 to 3.0 ± 0.3 and 4.0 ± 0.5 days when the ϕ_{PCL} increased from 31% to 70% and 90%. For SPL201 cells, the PI over seven days decreased from 5.4 ± 0.5 to 4.8 ± 0.6 and 2.6 ± 0.7 while the doubling time increased from 2.9 ± 0.2 to 3.1 ± 0.3 and 5.1 ± 1.4. We also examined rat bone marrow stromal cell attachment and proliferation on the crosslinked PPF-*co*-PCL disks and found the same trend with the composition (data not shown). In clear contrast with MC3T3-E1 and SPL201 cells, PC12 cells (Figure 4A(c,g,k),E) preferred crosslinked PPF-*co*-PCL disks with a higher ϕ_{PCL} as they proliferated better. By varying the ϕ_{PCL} from 31% to 70% and 90%, the PI of PC12 cells over four days increased from 3.3 ± 0.3 to 3.8 ± 0.3 and 4.0 ± 0.6 while the doubling time decreased from 2.3 ± 0.2 to 2.1 ± 0.1 and 2.0 ± 0.2.

MC3T3-E1 cell differentiation was characterized using two representative indicators at the onset of osteoblastic differentiation, the alkaline phosphatase (ALP) activity and calcium content of the cell lysates after seven-day culture. As shown in **Figure 5**A, both parameters decreased significantly with increasing the ϕ_{PCL} in the crosslinked PPF-*co*-PCL disks, consistent with the trends in other cell behaviors. To further analyze MC3T3-E1 cell differentiation, both reverse transcription (RT) and real-time polymerase chain reaction (PCR) were used to assess the expression levels of collagen I and osteocalcin relative to that of housekeeping glyceraldehyde-3-phosphate-dehydrogenase (GAPDH) in the total RNA extracted from the cells cultured on the substrates for two days and two weeks. Because MC3T3-E1 cells still proliferated at day 2, the relative expression levels of collagen I on all the disks were much higher than those at longer time of two weeks, while those of osteocalcin, one of the mature bone-specific markers for osteoblastic differentiation during mineralization, were much higher at week 2. Nevertheless, the role of copolymer composition in regulating expression of both gene markers was evident when they were at the higher levels. As demonstrated in Figure 5B,C, the expression levels of collagen I at day 2 and osteocalcin at week 2 were both significantly higher on the stiffer crosslinked PPF-*co*-PCL (ϕ_{PCL} = 31%) disks.

The images of NGF-differentiated PC12 cells in Figure 4A-d,h,l were quantified into three parameters: percentage of cells bearing neurites, neurite length, and number of neurites per cell. These three indicators of PC12 cell differentiation all increased with the ϕ_{PCL}, as summarized in Figure 5D. These observations strengthen our impression that cell–biomaterial interaction profiles need to be determined for each cell–material pair that is considered for a tissue engineering application, and that it may be possible to exploit these interaction profiles to affect selective cell retention of a desired cell type on a specific material surface.[7]

The chemical, topological, and mechanical properties of a material surface are three factors that can be manipulated to affect specific desired cell–material interactions.[29] In this study, the MC3T3-E1, SPL201, and PC12 cells behaved differently as the surface stiffness of the polymer disks changed. The crosslinked PPF-*co*-PCL disks in this study were fabricated between two glass plates and their gel fractions were all close to 100%. Thus, their smooth topology, found on scanning electron microscopic (SEM) images, was expected. This surface topology can be controlled by varying both the surface roughness of the mold and the crystallinity of the polymer. The polymer's hydrophilicity affects its capability to adsorb protein, and thus its function in vivo. The contact angle of water (Figure S9, Supporting Information) had a weak dependence on ϕ_{PCL}, ranging from 63° to 76°. The concentration of proteins adsorbed from the culture medium (Figure S10, Supporting Information) increased when ϕ_{PCL} increased. A possible explanation for this observation is that the hydrophilicity increased as ϕ_{PCL} increased, as also observed on crosslinked PPF/PCLF disks.[15] There is evidence that surfaces with a contact angle of ≈50° and a corresponding capability of adsorbing protein encourage cell attachment and proliferation,[29] although there are other studies which refute this association.[13,15,30] Those studies suggest that the amount of adsorbed proteins may not be the only factor that predicts cell affinity, since the adsorbed proteins may adopt different conformations on the surfaces in response to different local environments, and thus behave differently.[13] Nevertheless, differences in the scaffold's surface chemistry and topological features did not correlate with observed differences in cell attachment and proliferation on crosslinked PPF-*co*-PCLs with various compositions. In contrast, the observed trends in cell proliferation and morphology were consistent with differences in scaffold mechanical properties, specifically, surface stiffness.

The role of surface stiffness in regulating cell responses has been discovered for protein-coated hydrogels with different mechanical properties, which were achieved by varying the crosslinking density.[7–12] There are also studies that address this issue in hydrophobic polymers.[13–23,27] Stiffer hydrogels were reported to better support focal adhesion, spreading, proliferation, and differentiation of MC3T3-E1 cells and human mesenchymal stem cells.[31,32] For nerve cells, soft substrates can stimulate neurite extension and branching while inhibit glial cell spreading and proliferation, although mechanism of regulation is still under investigation.[10,11,33,34] SPL201 cells can differentiate into early Schwann cell-like cells, which are glial cells.[28] Consistent with the earlier reports on culturing glial cells on hydrogels, SPL201 cell proliferation was found to be enhanced on more rigid substrates, although the stiffnesses of our hydrophobic PPF-*co*-PCL networks were much higher than those of hydrogels (normally <1 MPa).[8–12] Strikingly, the higher proliferation and differentiation of neuronal-like PC12 cells on the weaker crosslinked PPF-*co*-PCL (ϕ_{PCL} = 90%) offered further rationale of using this material for nerve regeneration, in addition to the suitable mechanical properties. In contrast with the weaker hydrogels that had to be incorporated with polycations such as poly(L-lysine), matrigel, or adhesive proteins to allow cell attachment,[8–12] the hydrophobic PPF-*co*-PCL scaffolds evaluated here did not contain any postfabrication treatments such as protein coating or surface charge modification. In addition, the degree of crosslinking, which determines the distribution between crystalline and amorphous polymer domains, can be varied to optimize two important properties of nerve conduits: suture pull-out strength and conduit flexibility. Cell attachment and proliferation were greater on scaffolds that had lower crosslinking densities (less photoinitiator BAPO was used), and scaffolds that had ϕ_{PCL} > 90% had higher strengths.

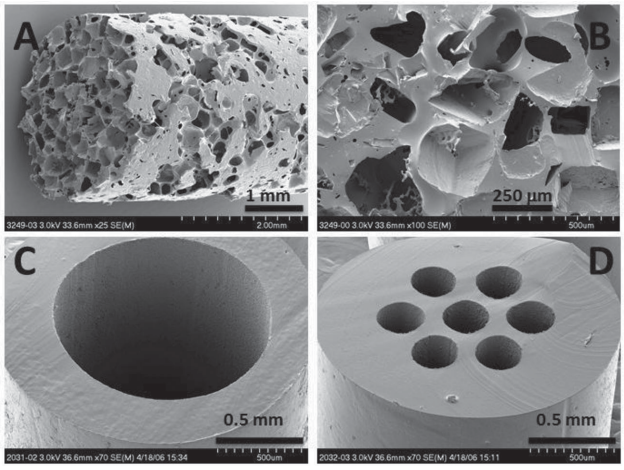

Figure 6. SEM images of crosslinked PPF-*co*-PCL bone scaffold and nerve conduits. A,B) A typical bone scaffold fabricated from PPF-*co*-PCL (ϕ_{PCL} = 31%) using salt-leaching technique; A) ×25, B) 100×. C) Single-lumen (×70) and D) seven-channel nerve conduits (×70) fabricated from PPF-*co*-PCL (ϕ_{PCL} = 90%). The scale bars represent A) 1, B) 0.25, C) 0.5, and D) 0.5 mm.

The nerve conduit must be strong enough to hold a suture during its insertion into the nerve defect, and it must maintain its circular cross-section when it crosses a joint and bends during joint motion. The increased mechanical properties are thought to occur because the percentage of crystalline domains in the scaffold increases as the ϕ_{PCL} increases.[27] Examples of these optimization strategies for bone regeneration and nerve regeneration include the fabrication of 3D PPF-*co*-PCL (ϕ_{PCL} = 31%) porous bone scaffolds with a porosity of 80% and pore size of 300–400 µm (**Figure 6**A,B). These scaffolds had strength, porosity, and connectivity designed to optimize load bearing capacity and osteoblast migration into the pores. The nerve regeneration scaffolds consisted of PPF-*co*-PCL (ϕ_{PCL} = 90%) and were fabricated into single-lumen and seven-channel conduits (Figure 6C,D). The polymeric composition selection criteria for making devices to address these two applications are that the devices have appropriate mechanical properties for their intended application and that they support cell attachment, proliferation, and differentiation for the cell type needed for each application. Crosslinked PPF-*co*-PCL (ϕ_{PCL} = 90%) nerve conduits supplied sufficient pull-out force, flexibility, suturability, and showed little swelling in vivo.

Figure 7 shows the histologic analysis of coronal sections prepared from scaffolds that had been implanted in a rat femoral bone defect for eight weeks. All polymer scaffolds maintained their original shape. Figure 7A shows that the scaffolds were surrounded by the original defect margins and fibrous tissue. Figure 7B is a higher magnification image that shows a

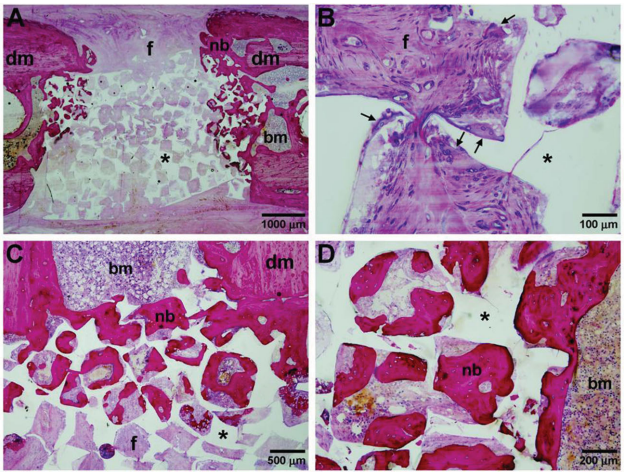

Figure 7. Coronal sections of a crosslinked PPF-*co*-PCL (ϕ_{PCL} = 31%) scaffold implanted in a rat femoral bone defect for eight weeks. Stained with methylene blue and basic fuchsin. nb = new bone; dm = defect margins; f = fibrous connective tissue; bm = bone marrow; * = scaffold; arrow = giant cells. The scale bars represent A)1000, B) 100, C) 500, and D) 200 µm.

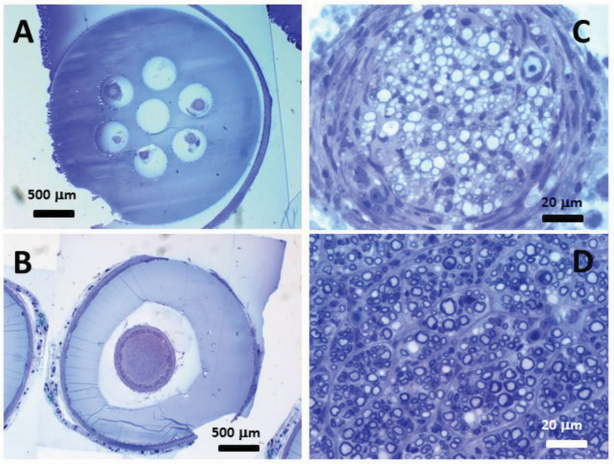

Figure 8. Cross sections taken from the middle part of crosslinked PPF-*co*-PCL nerve conduits. A,C) A crosslinked PPF-*co*-PCL (ϕ_{PCL} = 90%) seven-channel nerve conduit after four weeks of implantation [A) ×32, C) ×800] and B,D) a crosslinked PPF-*co*-PCL (ϕ_{PCL} = 90%) single-lumen nerve conduit after 16 weeks of implantation [B) ×32, D) ×800]. Stained with toluidine blue. The scale bars represent A,B) 500 µm and C,D) 20 µm.

mild foreign body reaction to the implanted material. This reaction consisted of inflammatory cells inside the scaffold pores, and macrophages and giant cells at the polymer–tissue interface. Figure 7C shows that newly formed bone extended from the original femur edges into the defect, and that the majority of the defects were filled with fibrous tissue. Figure 7D shows that the bone had a woven appearance, with osteocytes inside the matrix and lining the bone surfaces. The bone density, bone mineral content, and bone volume in the scaffolds were 0.122 ± 0.005 g mm^{-2}, 0.028 ± 0.004 g, and 18.0 ± 8.9 mm^3, respectively. Control scaffolds with the same porosity and pore size made using PPF-*co*-PCL (ϕ_{PCL} = 90%) were squeezed and bent in the center and less extension of newly formed bone as the result of their more compliant characteristics, although the parameters about new bone discussed above were not significantly different compared with crosslinked PPF-*co*-PCL (ϕ_{PCL} = 31%) scaffolds. It should be noted that besides the material properties, pore geometry, size, and interconnectivity of porous bone scaffolds are also critical in determining the in vivo bone ingrowth. In addition, porous crosslinked PPF-*co*-PCL (ϕ_{PCL} = 31%) scaffolds might suffer more from being brittle than its solid substrates and PPF-*co*-PCL (ϕ_{PCL} = 90%) counterparts. More extensive in vivo studies using different PPF-*co*-PCLs are under investigation and scaffolds made with identical pore interconnectivity can serve for a better comparison. Not included in Figure 7, we have also investigated bone regeneration using crosslinked PPF-*co*-PCL (ϕ_{PCL} = 31%) scaffolds embedded with poly(lactide-*co*-glycolide) (PLGA) microspheres that contain recombinant human bone morphogenetic protein-2 (rhBMP-2), which can induce bone formation. This combination of a stiff polymeric matrix that demonstrates slow degradation, and microspheres that degrade more rapidly, formed a controlled release scaffold system that resulted in healed rat femur bone defects in eight weeks.

The second scaffold application addressed guided nerve regeneration. **Figure 8**A,B shows that the structures of both single-lumen and seven-channel nerve conduits remained intact after 4 and 16 weeks of implantation. In addition, there was only a small layer of fibroblast tissue around the conduits at those two time periods. Figure 8C,D is higher magnification images that show myelinated axons in the midpart of the nerve conduit channels. The 16-week implantation specimens had a total fascicular area of 0.3165 mm^2, 7566 myelinated fibers per nerve, and a myelinated fiber density of 23 903 per mm^2. The myelinated fibers ranged from 1.23 to 7.67 µm in diameter, and their average diameter was 3.42 µm. The axons ranged from 0.83 to 6.28 µm in diameter, and their average diameter was 2.40 µm. Therefore, the myelin thickness ranged from 0.063 to 1.12 µm, and its average value was 0.51 µm.

3. Conclusions

We have designed and investigated novel photocrosslinkable PPF-*co*-PCL copolymers to address two different clinical needs, and demonstrated the controllability of physical properties and cell behavior using this series of molecularly engineered biomaterials. After photocrosslinking, PPF-*co*-PCLs with different percent compositions of PCL have a wide range of thermal and mechanical properties to satisfy diverse requirements in hard and soft tissue replacements, represented by bone and nerve regeneration in this report. Crosslinked PPF-*co*-PCLs demonstrate high cell viability (≈100%) for mouse MC3T3-E1 cells, rat SPL201 cells, and rat PC12 cells compared to those same cells plated onto TCPS. Furthermore, scaffold surface stiffness correlates with cell attachment, phenotypic expression, proliferation, and differentiation for both bone and nerve cell types on crosslinked PPF-*co*-PCL disks. Stiffer crosslinked PPF-*co*-PCLs promote MC3T3-E1 and SPL201 cell proliferation better than polymers that have lower stiffness while the trend is opposite for PC12 cells. The evaluation of scaffold mechanical properties and cell proliferation capabilities results in the selection of two

PPF-*co*-PCLs compositions for the fabrication of bone scaffolds and nerve conduits. Crosslinked PPF-*co*-PCLs have promising characteristics for use in both bone regeneration and peripheral nerve repair. Appropriate mechanical properties and biocompatibility characteristics have been demonstrated in both in vitro and in vivo for these two applications by selection of a polymer composition that optimizes these properties for the needs of the particular application.

4. Experimental Section

Materials and Fabrication of Polymer Disks and Scaffolds: Fifteen PPF-*co*-PCLs with a variety of PCL compositions from 29% to 90% were used in crosslinking characterizations. The photoinitiator BAPO (IRGACURE 819) was a gift from Ciba Specialty Chemicals (Tarrytown, NY). Seventy-five microliters of BAPO/CH_2Cl_2 (300 mg/1.5 mL) solution were mixed with 500 μL PPF-*co*-PCL/CH_2Cl_2 solution (1.5 g/500 μL). To reveal the effect of BAPO/PPF-*co*-PCL ratio on the thermal and mechanical properties of the resulted PPF-*co*-PCL networks, a smaller amount (12.5 μL) of the BAPO/CH_2Cl_2 solution was also applied to the same amount of PPF-*co*-PCL/CH_2Cl_2 solution to prepare the comparison group. The PPF-*co*-PCL/BAPO/CH_2Cl_2 mixture was transferred into a mold formed by two glass plates (2.1 mm, thickness) and a Teflon spacer (0.37 mm, thickness). The filled mold was placed under UV light (λ = 315–380 nm) from a distance of ≈7 cm for 30 min to perform crosslinking. Strips and disks with different dimensions were cut from crosslinked PPF-*co*-PCL sheets for the experiments described above. In the fabrication of porous bone scaffolds, PPF-*co*-PCL (ϕ_{PCL} = 31%)/BAPO/CH_2Cl_2 solution and salt (sodium chloride) particles (300–400 μm sieved size range) with calculated amounts were mixed to reach the final scaffold porosity, i.e., the fraction of pore volume in total scaffold volume, of 80%. The mixture was squeezed into a glass tube and crosslinked under UV light for 30 min. Porous scaffolds (5 mm length × 3 mm diameter) with a porosity of 80% were obtained after the salt particles were leached away in water. In the fabrication of nerve conduits, PPF-*co*-PCL (ϕ_{PCL} = 90%)/BAPO/CH_2Cl_2 mixture was injected from a syringe into a mold formed by a glass tube, stainless steel wires, and Teflon end-caps.[27] The filled mold was rotated under UV light for 30 min and crosslinked PPF-*co*-PCL (ϕ_{PCL} = 90%) conduits were soaked in acetone for two days to remove the solvent, unreacted BAPO, and sol fraction before being dried in vacuum. Details about measurements of gel fraction, swelling ratios, thermal properties, mechanical properties, surface hydrophilicity, protein adsorption, hydrolytic degradation, and SEM images are supplied in the Supporting Information.

In Vitro Cell Attachment and Proliferation: Details about cell culture and cytocompatibility tests are supplied in the Supporting Information. Crosslinked PPF-*co*-PCL disks were sterilized in excess 80% ethanol solution overnight with gentle shaking. Dried disks were washed with PBS three times prior to their use in cell studies. Cell attachment at 4 h and proliferation in four or seven days were tested by seeding the cells at a density of 15 000 cells per cm^2 directly onto sterile crosslinked PPF-*co*-PCL disks, which were positioned on the well bottoms in 48-well tissue culture plates using sterilized inert silicon-based high temperature vacuum grease (Dow Corning, Midland, MI) to keep them in place. After one, four, and seven days, culture medium was removed and the polymer disks were washed with PBS twice. Cell density was evaluated by using the MTS assay kit (Promega, Madison, WI), and measuring the UV absorbance at 490 nm of the incubated polymer disk, solution, and attached cells. Cell morphology was assessed by fixing polymer disks and their attached cells paraformaldehyde (PFA) solution for 10 min. The cells were then washed twice with PBS and permeabilized with 0.2% Triton X-100. They were then stained using rhodamine–phalloidin for 1 h at 37 °C and 4′,6-diamidino-2-phenylindole dihydrochloride (DAPI, Thermo Scientific, Rockford, IL) at ambient temperature prior to photography using an Axiovert 25 Zeiss light microscope (Carl Zeiss, Germany). Additional vinculin focal adhesion staining was performed for MC3T3-E1 cells using monoclonal anti-vinculin antibody and fluorescein-isothiocyanate-labeled secondary antibody (FITC, Molecular Probes, Eugene, OR) as described previously.[35] Cell area was determined and averaged on 20 nonoverlapping cells at 4 h and day 1 postseeding using ImageJ software (National Institutes of Health, Bethesda, MD).

ALP Activity, Calcium Content, and Gene Expression in MC3T3-E1 Cells: The ALP activity and calcium content of MC3T3-E1 cells cultured on crosslinked PPF-*co*-PCL disks for seven days were measured using the method reported earlier.[16,35] The cells were washed twice with PBS, trypsinized, and washed again by centrifugation at 1000 rpm for 4 min. The residues were resuspended in 1 mL of 0.2% Nonidet P-40 and sonicated in an ice bath for 2 min. The cell lysate was frozen at −20 °C before the ALP activity of cell lysate was measured using a fluorescence-based ALP detection kit (Sigma, St. Louis, MO) and a standard curve constructed using different amounts of control enzyme. Calcium content was performed using QuantiChrom calcium assay kit (BioAssay Systems, Hayward, CA). MC3T3-E1 cells cultured on 50 cm^2 polymer sheets at 15 000 cells per cm^2 for two weeks were trypsinized and total RNA was isolated using RNeasy Mini Kit (Qiagen, Valencia, CA). The amount of total RNA from each sample was quantified using Nanodrop1000 spectrophotometer (Thermo Scientific, Wilmington, DE). Reverse transcription of isolated RNA was then performed using DyNAmo cDNA synthesis kit (Thermo Scientific) according to the manufacturer's protocol. The oligonucleotide primers used for both RT and real-time PCR were as follows: Collagen I forward, 5′-TCT CCA CTC TTC TAG TTC CT; Collagen I reverse, 5′- TTG GGT CAT TTC CAC ATG C; product size: 269 bp. Osteocalcin forward, 5′-CAA GTC CCA CAC AGC AGC TT; Osteocalcin reverse, 5′-AAA GCC GAG CTG CCA GAG TT; product size: 371 bp GAPDH forward, 5′-ACT TTG TCA AGC TCA TTT CC; GAPDH reverse, 5′-TGC AGC GAA CTT TAT TGA TG; product size: 267 bp. The detailed PCR procedures are supplied in the Supporting Information.

Differentiation of PC12 Cells: Attached PC12 cells on crosslinked PPF-*co*-PCL disks were treated with 50 ng mL^{-1} NGF in growth media to induce neurite outgrowth. Differentiated cells at day 7 were analyzed using the ImageJ. At least ten images were counted for the percentage of cells bearing neurites, the number of neurites per cell, and neurite length. Only neurites longer than the diameter of original, round PC12 cells (≈10 μm) were considered as positive neurite extension and cells with at least one neurite longer than 10 μm were counted as neurite-bearing cells.

In Vivo Implantation and Histological Evaluation: Pilot animal testing was performed according to a protocol approved by the Institutional Animal Care and Use Committee (IACUC) of Mayo Clinic. The bone scaffolds and nerve conduits were sterilized in 80% ethanol for 30 min and dried in vacuum overnight prior to implantation. Porous crosslinked PPF-*co*-PCL (ϕ_{PCL} = 31%) scaffolds were implanted in a critical sized rat femoral bone defect model. Four male Harlan Sprague Dawley rats (310–335 g, weight) were used. Anesthesia was performed by an intramuscular injection of a ketamine/xylazine mixture (45 mg/10 kg) and the surgical sites were shaved and disinfected. A 2-cm skin incision was made along the lateral site of the right limb to expose the femur, which was circumferentially freed from muscles. A predrilled polyethylene plate (22 mm length × 3 mm height × 4 mm width) was fixed to the femur with 1 mm Kirchner-wires (Zimmer, Warsaw, IN). Subsequently, a 5-mm segmental defect was created, which was filled with the porous crosslinked PPF-*co*-PCL (ϕ_{PCL} = 31%) scaffolds. After eight weeks, the rats were euthanized and the implants were excised and fixed in a 1.5% phosphate buffered glutaraldehyde solution. The implants were dehydrated in a graded series of alcohol and embedded in methylmethacrylate for histological analysis. Sections were stained with basic fuchsin and methylene blue for evaluating the general tissue response and bone formation.[36] The nerve implantation studies were done in a rat sciatic nerve defect model. The experimental design used 12 female Sprague Dawley rats. Six rats received a single lumen nerve guidance scaffold and six rats received a seven-channel nerve guidance channel. A 5 mm section of the sciatic nerve was removed beginning

at a point 5 mm distal to the tendon of the obturator internus muscle. The resected nerve segment was replaced with a crosslinked PPF-*co*-PCL (ϕ_{PCL} = 90%) conduit. The cut nerve ends were inserted ≈1 mm into either end of the conduit and held in place by sutures. The specimens were harvested after six weeks in vivo and fixed in situ for 30 min in trumps fixative (2% PFA and 1% glutaraldehyde in PBS, pH = 7.2) using published methods.[37] The samples were then embedded in methylmethacrylate, sectioned, stained with toluidine blue, and evaluated for the presence of myelinated axons, macrophages, and fibroblasts.

Statistical Analysis: Student's *t*-test was performed to assess the statistical significance ($p < 0.05$) of the differences between results.

Supporting Information

Supporting Information is available from the Wiley Online Library or from the author.

Acknowledgements

This work was supported by the Mayo Foundation and the NIH (Grant Nos. R01 AR56212 and R01 EB03060) for L.L. and M.J.Y., and the National Science Foundation (Grant No. DMR-11-06142) for S.W. D.H.R.K. thanks the support from the Netherlands Organization for Health Research and Development ZonMW (Agiko 920-03-325). We thank J. A. Gruetzmacher for the preparation of polymer disks, J. J. Nesbitt for SPL201 cell culture, and J. L. Lewis and N. K. Simha for their help with indentation.

Received: January 9, 2015
Revised: February 26, 2015
Published online: March 23, 2015

[1] Y. Khan, M. J. Yaszemski, A. G. Mikos, C. T. Laurencin, *J. Bone Jt. Surg. Am.* **2008**, *90A*, 36.
[2] M. J. Yaszemski, R. G. Payne, W. C. Hayes, R. Langer, A. G. Mikos, *Biomaterials* **1996**, *17*, 175.
[3] C. E. Schmidt, J. B. Leach, *Annu. Rev. Biomed. Eng.* **2003**, *5*, 293.
[4] S. Wang, L. Cai, *Int. J. Polym. Sci.* **2010**, 138686.
[5] S. Wang, L. Lu, J. A. Gruetzmacher, B. L. Currier, M. J. Yaszemski, *Macromolecules* **2005**, *38*, 7358.
[6] X. F. Shi, A. G. Mikos, *An Introduction to Biomaterials* (Eds: S. A. Guelcher, J. O. Hollinger), CRC Press, Boca Raton, FL **2006**, pp 205–218.
[7] D. E. Discher, P. Janmey, Y. L. Wang, *Science* **2005**, *310*, 1139.
[8] R. J. Pelham, Jr. , Y.-L. Wang, *Proc. Natl. Acad. Sci. U.S.A.* **1997**, *94*, 13661.
[9] I. Levental, P. C. Georges, P. A. Janmey, *Soft Matter* **2007**, *3*, 299.
[10] S. Nemir, J. L. West, *Annu. Biomed. Eng.* **2009**, *38*, 2.
[11] L. A. Flanagan, Y.-E. Ju, B. Marg, M. Osterfield, P. A. Janmey, *NeuroReport* **2002**, *13*, 2411.
[12] L. Cai, J. Lu, V. Sheen, S. Wang, *Biomacromolecules* **2012**, *12*, 342.
[13] X. Q. Brown, K. Ookawa, J. Y. Wong, *Biomaterials* **2005**, *26*, 3125.
[14] Y. Mei, K. Saha, S. R. Bogatyrev, J. Yang, A. L. Hook, Z. I. Kalcioglu, S Cho, M. Mitalipova, N. Pyzocha, F. Rojas, K. J. Van Vliet, M. C. Davies, M. R. Alexander, R. Langer, R. Jaenisch, D. G. Anderson, *Nat. Mater.* **2010**, *9*, 768.
[15] S. Wang, D. H. Kempen, N. K. Simha, J. L. Lewis, A. J. Windebank, M. J. Yaszemski, L. Lu, *Biomacromolecules* **2008**, *9*, 1229.
[16] L. Cai, J. Chen, A. Rondinone, S. Wang, *Adv. Funct. Mater.* **2012**, *22*, 3181.
[17] L. Cai, K. Wang, S. Wang, *Biomaterials* **2010**, *31*, 4457.
[18] K. Wang, L. Cai, S. Wang, *Polymer* **2011**, *52*, 2827.
[19] K. Wang, L. Cai, F. Hao, X. Xu, M. Cui, S. Wang, *Biomacromolecules* **2010**, *11*, 2748.
[20] L. Cai, S. Wang, *Polymer* **2010**, *51*, 164.
[21] L. Cai, S. Wang, *Biomaterials* **2010**, *31*, 7423.
[22] K. Wang, L. Cai, L. Zhang, J. Dong, S. Wang, *Adv. Healthcare Mater.* **2012**, *1*, 292.
[23] L. Cai, L. Zhang, J. Dong, S. Wang, *Langmuir* **2012**, *28*, 12557.
[24] S. Wang, M. J. Yaszemski, J. A. Gruetzmacher, L. Lu, *Polymer* **2008**, *49*, 5692.
[25] R. Murugan, S. Ramakrishna, *Compos. Sci. Technol.* **2005**, *65*, 2385.
[26] G. H. Borschel, K. F. Kia, W. M. Kuzon, R. G. Dennis, *J. Surg. Res.* **2003**, *114*, 133.
[27] S. Wang, M. J. Yaszemski, A. M. Knight, J. A. Gruetzmacher, A. J. Windebank, L. Lu, *Acta Biomater.* **2009**, *5*, 1531.
[28] C. S. Lobsiger, P. M. Smith, J. Buchstaller, B. Schweitzer, R. J. Franklin, U. Suter, V. Taylor, *Glia* **2001**, *36*, 31.
[29] G. M. Harbers, D. W. Grainger, *An Introduction to Biomaterials* (Eds: S. A. Guelcher, J. O. Hollinger), CRC Press, Boca Raton, FL **2006**, pp 15–45.
[30] B. Saad, O. M. Keiser, M. Welti, G. K. Uhlschmid, P. Neuenschwander, U. W. Suter, *J. Mater. Sci.: Mater. Med.* **1997**, *8*, 497.
[31] C. B. Khatiwala, S. R. Peyton, A. J. Putnam, *Am. J. Physiol. Cell. Physiol.* **2006**, *290*, 1640.
[32] R. A. Marklein, J. A. Burdick, *Soft Matter* **2010**, *6*, 136.
[33] P. C. Georges, W. J. Miller, D. F. Meaney, E. S. Sawyer, P. A. Janmey, *Biophys. J.* **2006**, *90*, 3012.
[34] A. Kostic, J. Sap, M. P. Sheetz, *J. Cell Sci.* **2007**, *20*, 3895.
[35] X. Wu, S. Wang, *ACS Appl. Mater. Interfaces* **2012**, *4*, 4866.
[36] D. H. R. Kempen, L. Lu, T. E. Hefferan, L. B. Creemers, A. Maran, K. L. Classic, W. J. A. Dhert, M. J. Yaszemski, *Biomaterials* **2008**, *29*, 3245.
[37] G. C. de Ruiter, R. J. Spinner, M. J. A. Malessy, M. J. Moore, E. J. Sorenson, B. L. Currier, M. J. Yaszemski, A. J. Windebank, *Neurosurgery* **2008**, *63*, 144.